Int. J. Electrochem. Sci., 14 **(2019)** 5096 – 5106, doi: 10.20964/2019.06.19

International Journal of
ELECTROCHEMICAL
SCIENCE
www.electrochemsci.org

Porous N-doped Carbon Derived from ZIF-8/Reduced Graphene oxide/Polypyrrole Composite for High Performance Supercapacitor

Yin Liu[1], *Qingli Sui*[1], *Yongjin Zou*[1,2], *Cuili Xiang*[1,*], *Fen Xu*[1], *Jingjing Xie*[3], *Lixian Sun*[1,*]

[1]Guangxi Key Laboratory of Information Materials, Guilin University of Electronic Technology, Guilin 541004, P.R. China
[2]School of Chemistry and Chemical Engineering, Hunan University of Science and Technology, Xiangtan, 411201, China
[3]State Key Laboratory of Advanced Technology for Materials Synthesis and Processing, Wuhan University of Technology, Wuhan, 430070, China
[*]E-mail: xiangcuili@guet.edu.cn, sunlx@guet.edu.cn

Received: 6 January 2019 / *Accepted:* 10 March 2019 / *Published:* 10 May 2019

Porous N-doped carbon nanomaterials have great potential in supercapacitor owing to their high surface area, excellent chemical stability and good hydrophilic property. In this work, ZIF-8 nanocystals were well grown on the surface of polypyrrole/reduced graphene oxide composite (ZIF-8/PPy/rGO). After carbonization of ZIF-8/PPy/rGO and chemical etching of the product, a porous carbon with N-doping (PNC) and proper structure was obtained. In comparison with the carbonized ZIF-8 and PPy/rGO, the ZIF-8/PPy/rGO derived carbon possesses much higher electrochemical performance. As electrodes in supercapacitor, the PNC exhibits a significantly enhanced specific capacitance (236 F g^{-1} at 1 A g^{-1}), superior rate capability (retained 86.1 % from 1 to 20 A g^{-1}) and excellent cycling stability (over 96.8% capacity retained after 10000 cycles), exhibiting its potential for electrode materials with high performance.

Keywords: ZIF-8; Supercapacitor; Porous carbon; Graphene; N-doping

1. INTRODUCTION

As a new energy storage device, supercapacitor has raised much attention in recent years[1-4]. It possesses high power density, light weight, excellent cycling stability and short rechargeable time. The electrode material is the core component of the supercapacitor, which determines most of the performance of the supercapacitor. Carbonaceous materials are widely used for supercapacitor because of their good chemical stability, highly porous structure and large pore volume. So far, many porous

carbons derived from various carbon sources have been fabricated [5-8]. However, the electrochemical performance of the supercapacitor not only relies on the surface area of the electrode materials, but also the appropriate pore structure and conductivity [9-11]. For instance, the activated carbon has super high surface area [12-16], but the capability of charge storage is not very good. Therefore, design of carbon materials with unique structure is highly desirable for a supercapacitor [17-21].

It is well known that doping of heteroatom in the backbone of carbon materials can significantly enhance the performance of the supercapacitor [22]. MOFs provide such a unique capability due to their abundance of heteroatom containing and super high large surface area [23, 24], which are ideal precursors for architecting the carbon materials. However, the synthesis of MOFs-derived porous carbons requires some expensive templates, which lead to poor carbon structure. To this end, graphene, a two-dimensional single layer carbon with high conductivity has been regarded as the promising candidate [25-31].

In this study, we developed a facile, scalable, inexpensive method to synthesis a hierarchical porous N-doped carbon (PNC). Pyrrole was firstly polymerized on the surface of graphene to reduce the aggregation of the particles. Then ZIF-8 was then grown on the surface of the PPy/rGO nanocomposite. The ZIF-8/PPy/rGO composite was enlisted as a precursor to prepare the sandwiched PNC. During the carbonization of ZIF-8/PPy/rGO composite, the porous structure of ZIF-8 was well retained. The obtained PNC demonstrated excellent electrochemical performance, which is promising to be used in energy storage devices.

2. MATERIALS AND METHODS

2.1. Chemicals and Methods

Reduced graphene oxide (rGO) was prepared with Hummers' method [32]. ZIF-8, cetyltrimethylammonium bromide and pyrrole were purchased from Sigma–Aldrich (China).

The preparation of PPy/rGO was carried out by in-situ chemical polymerization. In a typical process, 0.1 g of rGO was added to 100 mL water and ultrasonicated for 1 h. Next, 1 mL of pyrrole and 0.1 g of cetyltrimethylammonium bromide was added to the suspension under stirring. Then 10 ml of ammonium persulfate solution (0.2 g/mL) was added to the above mixture dropwisely. The mixture was vigorously stirred for 2 h. Finally, the precipitation was filtered, completely washed and dried in an oven for 24 h.

To prepare ZIF-8/PPy/rGO, 0.1 g of PPy/rGO and 1.34 g $Zn(NO_3)_2 \bullet 6H_2O$ was firstly added to 120 mL of methanol, followed by the addition of 2-methylimidazole solution (0.74 g in 10 ml methanol) dropwisely under stirring [33]. The suspension solution was held at room temperature for 24 h and then filtered and washed with methanol. The solid was dried in an oven under vacuum for 24h.

PNC was obtained by pyrolysis of ZIF-8/PPy/rGO under N_2 at 800 °C for 4 h. The black powder was etched with 37% HCl for 24 h and then dried at 80 °C. The final product was recognized as PNC. As comparison, ZIF-8 and PPy/rGO were also carbonized with the same conditions and denoted as ZIF-C and PPy/rGO-C, respectively.

2.2. Characterization

The morphology of samples was analyzed using a FEI Quanta200 scanning electron microscope (SEM). The transmission electron microscopy (TEM) was obtained on a FEI Tecnai F20 microscope. The powder X-ray diffraction (XRD) pattern measurements were recorded using an 1820 Philips diffractometer. The textural properties of the samples were examined by N_2 adsorption/desorption measurements using a Quantachrome Autosorb-iQ2 Automated gas sorption system at 77 K.

2.3. Electrochemical tests

To examine the capacitive properties of PNC, the working electrodes were prepared by pressing the slurry made up of 85% of electroactive material, 10% of carbon black and 5% of poly (tetrafluoroethylene) (PTFE) binder onto nickel-foam (1 × 1 cm^2) current collectors. Then the electrodes were dried in an oven at 60 °C for 2 h. Cyclic voltammetry (CV) and galvanostatic charging-discharging (GCD) measurements were carried out using a CHI660E electrochemical workstation with a three electrode configuration (the electroactive material loaded nickel-foam as a working electrode, platinum foil as a counter electrode and Ag/AgCl as a reference electrode) in 6 M KOH.

3. RESULTS AND DISCUSSION

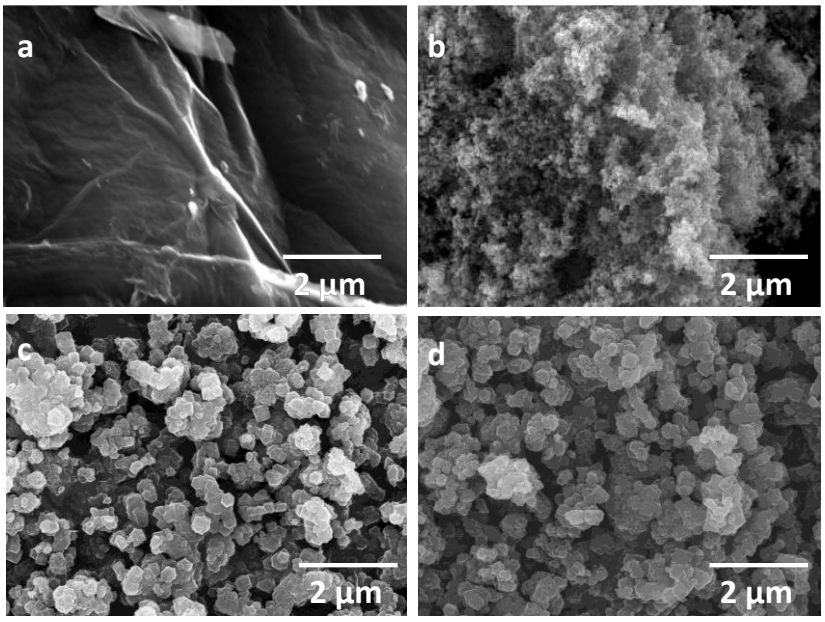

Figure 1. SEM images of rGO (a), PPy/rGO (b), ZIF-8/PPy/rGO (c) and PNC (d).

The microstructures of the prepared samples were observed by SEM. The SEM image of reduced graphene oxide demonstrates typical wrinkled surface (Figure 1a). After the polymerization of pyrrole, the surface becomes rough (Figure 1b). The polymerization of pyrrole not only inhibit the restacking the graphene, but also offer large accessible surface area for electrolyte. The ZIF-8 particles

with a size of 80-100 nm are well anchored on the surface of PPy/rGO (Figure 1c). After the carbonization of ZIF-8/PPy/rGO, the shape of ZIF-8 particles was well kept (Figure 1d), indicating the effective prevention of carbon nanoparticles during calcination process.

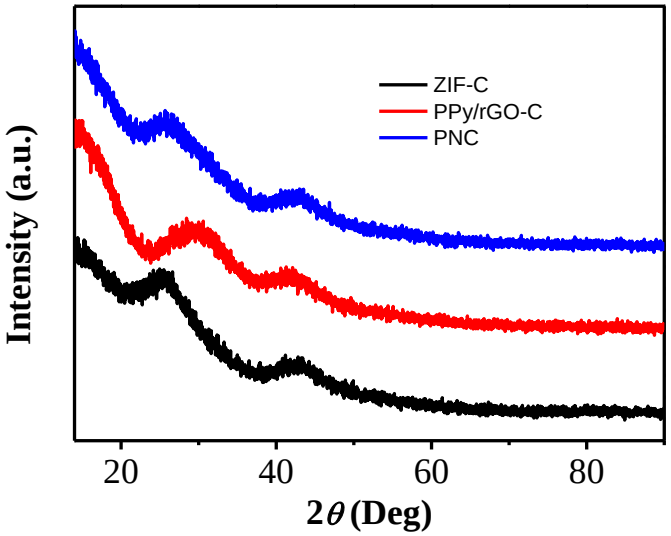

Figure 2. XRD patterns of PNC, PPy/rGO-C and ZIF-C.

The powder XRD patterns of PNC, PPy/rGO-C and ZIF-C are shown in Figure 2. A featured peak at 2θ=25.7°, 29.5°, 26.4° was observed for ZIF-C, PPy/rGO-C and PNC, respectively. The peaks are broad for all the samples, indicating the signature of amorphous carbon. The other diffraction peak was observed at around 43.1°, corresponding the (101) plane of amorphous carbon.

Figure 3 depicts the XPS spectra of PNC. The survey spectrum shows only three peaks corresponding to C, N, and O (Figure 3a), indicating the Zn species was successfully removed from the product. The chemical binding states of C, N, and O were further analyzed by deconvoluting their core level. The C 1s signal in Figure 3b can be deconvolved into four peaks. The peak located at 284.5 eV is corresponding to the C=C graphitic carbon. A deconvoluted peak observed at a binding energy of 285.1 eV in the C1s core level spectra of PNC is attributed to sp^2 carbon bonded to nitrogen or oxygen. Another peak located at a binding energy of 287.86 eV is indexed to sp^3 hybridized carbon. The fourth peak located at 288.5 eV can be indexed to the carbon singly bonded to terminal nitrogen. The signals of N 1s located at 398.5, 400.1 , 400.9 and 403.2 eV are attributed to the pyridinic N, pyrrolic N, quatenary N and pyridine N oxide, respectively (Figure 3c) [34]. It is well known that the N doping in the carbon back can contribute to the capacitance by Faradaic reactions [35]. Finally, the O 1s spectrum is also shown in Figure 3d, and the three peaks at 529.6, 531.4, and 533.1 eV are attributed to C-O, C=O, and N-O, respectively. The rich oxygen-containing functional groups still remain after the thermal treatment, which is beneficial to hydrophilicity [36].

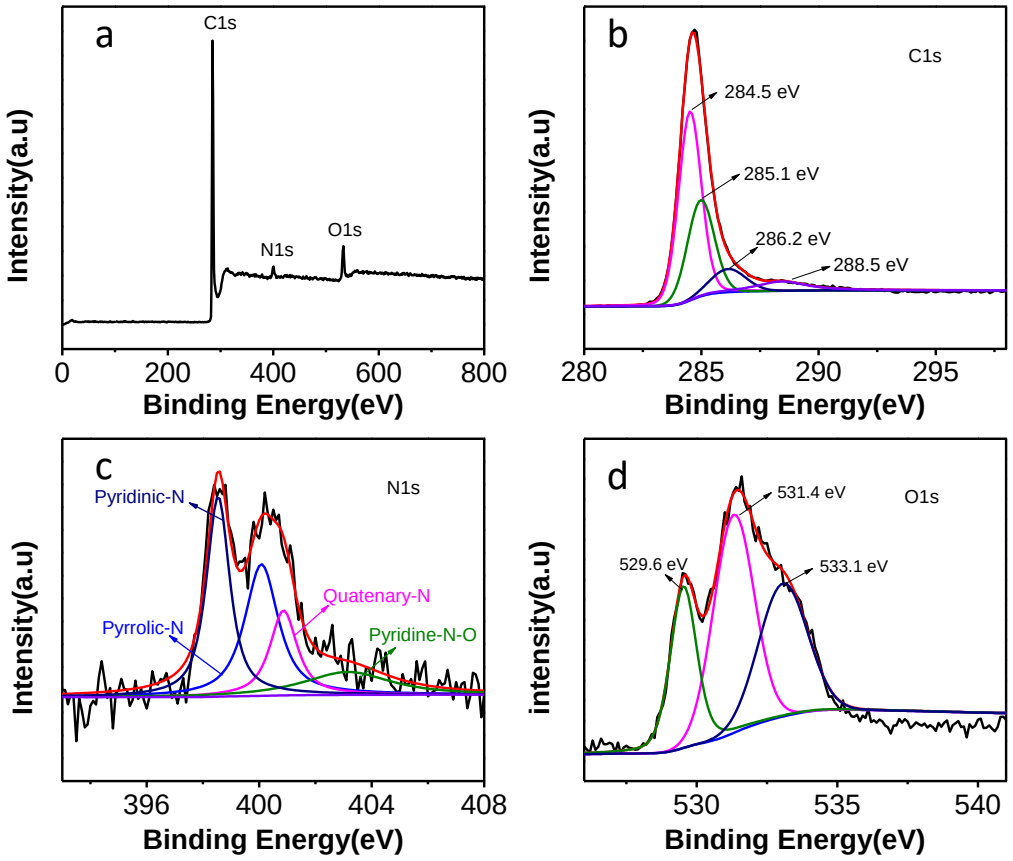

Figure 3. (a) XPS survey spectrum, (b) C1s high-resolution spectrum, (c) N1s high-resolution spectrum and (d) O1s high-resolution spectrum.

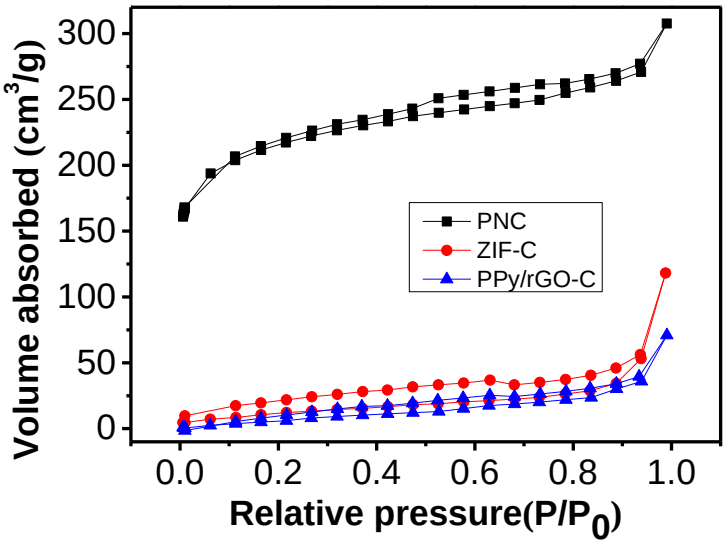

Figure 4. Nitrogen sorption isotherms of PNC, ZIF-C and PPy/rGO-C.

The nitrogen adsorption/desorption isotherms were further used to understand the textural properties of the as-synthesized samples. As shown in Figure 4, all the samples exhibit type-IV isotherm, a characteristic of mesoporous materials. PNC exhibits a wider hysteresis loop than

PPy/rGO-C and ZIF-C, which indicates that PNC possesses a higher number of mesopores than the other two samples. The calculated BET surface areas are 38.6, 67.2 and 169.2 m^2/g for PPy/rGO-C, ZIF-C and PNC, respectively. PNC demonstrates the highest surface area among the three samples, which is expected to deliver better capacitance properties than the other two samples.

3.2 Electrochemical characterization of PNC

The electrochemical behavior of the PNC was investigated by GCD cycling and CV. The GCD cycles at a current density of 1 A g^{-1} are shown in Figure 5. Though the charge-discharge cycles of all samples show a linear change in potential with time during charging and discharging, the time is different. The specific capacitance values calculated from the discharge curve of samples follow this order: PNC (236 F g^{-1}) > ZIF-C (98 F g^{-1}) > PPy/rGO-C (72 F g^{-1}). The highest value of specific capacitance obtained for PNC as compared to ZIF-C and PPy/rGO-C is attributed to its higher surface area, more number of mesopores and larger pore volume. Besides, the relatively high percentage of the carbonyl group in PNC could have also contributed to the measured capacitance by Faradaic reaction. As listed in Table 1, the capacitance of PNC electrode is comparable with the carbon-based materials, which demonstrates the superiority of PNC.

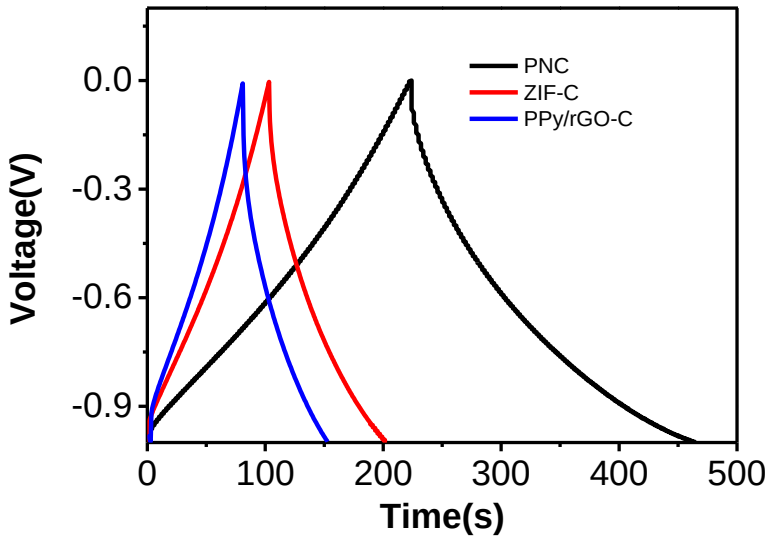

Figure 5. GCD cycles recorded at a current density of 1 A g^{-1} of PNC, PPy/rGO-C and ZIF-C in 6 M KOH electrolyte.

Figure 6 shows the GCD curve of PNC at different current density. The PNC electrode performed specific capacitance of 236, 224.2, 214.2, 210.1, and 203.2 F g^{-1} at current densities of 1, 2, 5, 10, and 20 A g^{-1}, respectively. As the current density increased from 1 to 20 A g^{-1}, there is a good rate capability (86.1% retention rate).

Table 1. Comparison of specific capacitance of PNC with previous reported carbon materials

Sample	Current density ($A\ g^{-1}$)	Specific capacitance ($F\ g^{-1}$)	Reference
ZIF-L@ZIF-8	1	274	[33]
PNCs-C8	1	245	[36]
CNC@ZIF-8-C	0.1	172	[37]
PC-CNTs	0.1	250	[38]
PC1000@C	0.5	225	[39]
NCGs	0.5	225	[40]
PNCs/rGO-800	1	245	[41]
ZIF-8@ZnO	1	290	[42]
ZIF7/CNF	1	202	[43]
PNC	1	236	This work

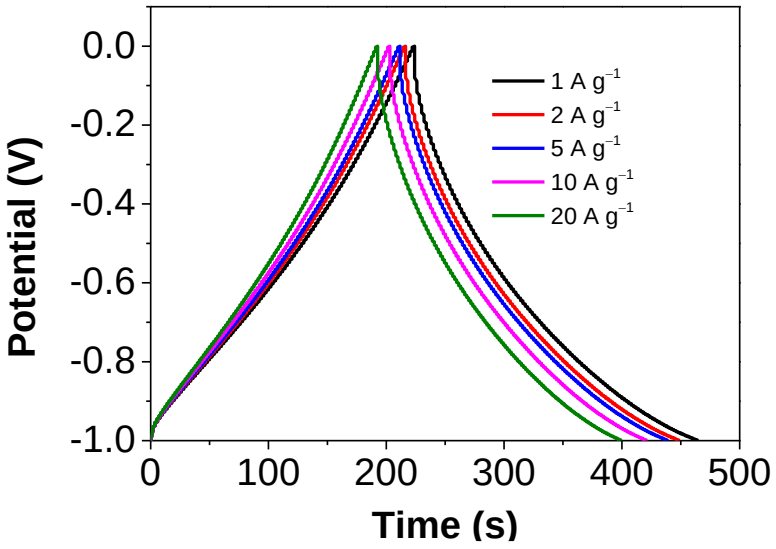

Figure 6. GCD curves of the PNC at the density of 1, 2, 5, 10 and 20 A/g.

CVs were recorded at various scan rates and are presented in Figure 7. As expected, all the PNC samples show a progressive increase in current response on increasing the scan rate. Although all the samples retain their quasi-rectangular shape up to 100 mV s^{-1}, they show a slight deviation when cycled beyond 100 mV s^{-1}, which suggests that the materials exhibit relatively lower capacitive storage performance at higher scan rates. This observation could be attributed to the decrease in the time taken for the effective interaction between the ions from the electrolyte and the electroactive sites of the materials at the higher scan rate [44-47].

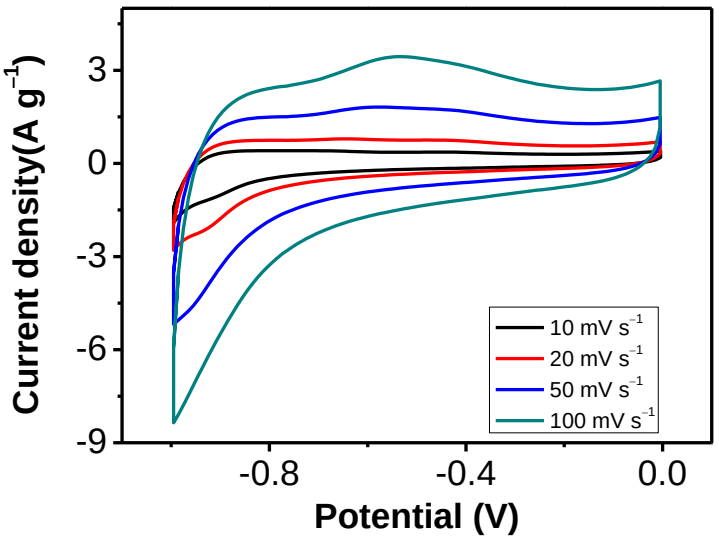

Figure 7. CV curves of the PNC at scan rates of 10, 20, 50 and 100 mVs^{-1}.

A symmetric two-electrode cell was further assembled to investigate the practical application of the PNC material. As shown in Figure 8, the symmetric cell demonstrates a high specific capacitance of 78.1 F g^{-1} at a current density of 1 A g^{-1}. From the GCD curve at different current density, the energy density and power density can be calculated. The symmetric cell shows a high energy/power density (12.8 Wh kg^{-1} at 227.1 W kg^{-1}). The structure of the material was well optimized by the combination of graphene, polypyrrole and ZIF-8. The ions transportation was facilitated in the materials, which improved the performance of the composite significantly [48-52].

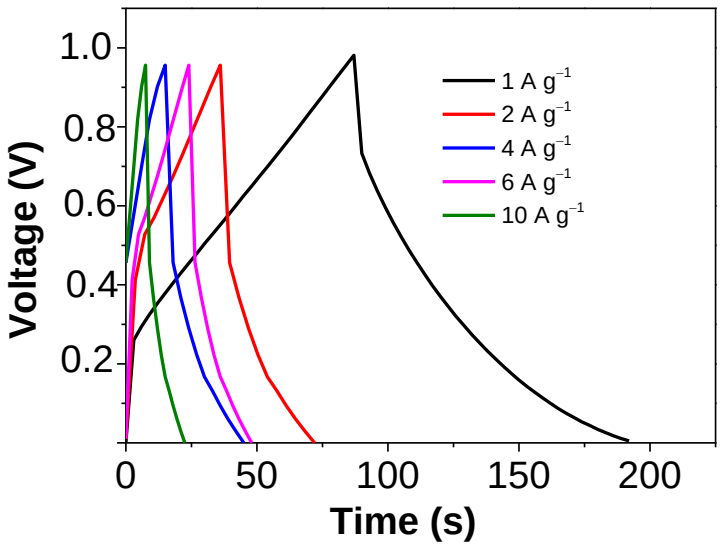

Figure 8. GCD curves of the PNC symmetric two-electrode cell at the current density of 1, 2, 4, 6 and 10 A/g.

The cycling stability is an important parameter the supercapacitor, which determines the

possibility of the application directly. In this study, the PNC symmetric cell was charged and discharged for 10000 cycles (Figure 9). The symmetric cell can retain 96.8% of the initial capacitance after 10000 cycles, demonstrating an excellent stability.

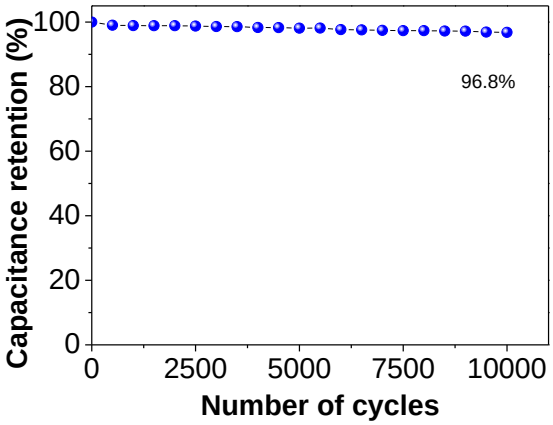

Figure 9. Cycling stability of the PNC symmetric supercapacitor at the current density of 1 A g^{-1}.

4. CONCLUSIONS

Porous N-doped carbon was facilely prepared by the carbonization of ZIF-8/PPy/rGO nanocomposite. The unique sandwiched structure of PNC enables the fast ion transport and excellent electrochemical performance. A specific capacitance of 236 F g^{-1} was obtained at the current density of 1 A g^{-1} for the PNC electrode. A PNC symmetric two-electrode cell was further assembled to investigate the practical using. The assembled PNC symmetric two-electrode cell exhibits high energy density and the capacity maintains 96.8% of initial capacity after 10000 cycles.

ACKNOWLEDGEMENTS
This work was supported by the Guangxi undergraduate innovation and entrepreneurship training program (201810595017) and GXNSF (2016GXNSFFA380012, 2017AD23029, 2017GXNSFDA198018).

References

1. K. Deng, C. Li, X. Qiu, J. Zhou, Z. Hou, *Electrochim. Acta*, 174(2015)1096-1103.
2. Z. Deng, Q. Yi, Y. Zhang, H. Nie, *J. Electroanal. Chem.*, 803 (2017) 95-103.
3. G.R. Xu, Y. Wen, X.P. Min, W.H. Dong, A.P. Tang, H.S. Song, *Electrochim. Acta*, 186 (2015) 133-141.
4. H. Yan, T. Li, K. Qiu, Y. Lu, J. Cheng, Y. Liu, J. Xu, Y. Luo, *J. Solid State Electrochem.*, 19 (2015) 3169-3175.
5. L. Bao, B. Liu, X. Li, C. Pan, Y. Xie, X. Lu, *Dalton T.*, 45 (2016) 11606-11610.
6. J. Chen, Y. Li, K. Lv, W. Zhong, H. Wang, Z. Wu, P. Yi, J. Jiang, *Sens. Actuators B-Chem.*, 224 (2016) 298-306.
7. S. Chen, L. Zhang, Y. Long, F. Zhou, *Electroanal.*, 26 (2014) 1236-1248.

8. K. Deng, C. Li, H. Huang, X. Li, *Sens. Actuators B-Chem.*, 238 (2017) 1302-1308.
9. K. Deng, C. Li, X. Qiu, J. Zhou, Z. Hou, *J. Electroanal. Chem.*, 755 (2015) 197-202.
10. K. Deng, J. Zhou, X. Li, *Electrochim. Acta*, 114 (2013) 341-346.
11. B. Liao, W. Wang, P. Long, X. Deng, B. He, Q. Liu, S. Yi, *Carbon*, 91 (2015) 30-37.
12. B. Liao, P. Long, B. He, S. Yi, Q. Liu, R. Wang, *Carbon*, 73 (2014) 155-162.
13. J. Liu, C. Zhang, T.W. Rees, L. Ke, L. Ji, H. Chao, *Coordin. Chem. Rev.*, 363 (2018) 17-28.
14. M. Tang, Y. Yang, S. Zhang, J. Chen, J. Zhang, Z. Zhou, Q. Liu, *Inorg. Chem.*, 57 (2018) 277-287.
15. Z. Wang, B. Zheng, H. Liu, X. Lin, X. Yu, P. Yi, R. Yun, *Cryst. Growth Des.*, 13 (2013) 5001-5006.
16. Z. Wang, B. Zheng, H. Liu, P. Yi, X. Li, X. Yu, R. Yun, *Dalton T.*, 42 (2013) 11304-11311.
17. L. Yi, W. Wei, C. Zhao, C. Yang, L. Tian, J. Liu, X. Wang, *Electrochim. Acta*, 158 (2015) 209-218.
18. Q. Yi, W. Huang, J. Zhang, X. Liu, L. Li, *Catal. Commun.*, 9 (2008) 2053-2058.
19. S. Zhang, H. Li, E. Duan, Z. Han, L. Li, J. Tang, W. Shi, P. Cheng, *Inorg. Chem.*, 55 (2016) 1202-1207.
20. X. Zhang, J. Xu, H. Wang, J. Zhang, H. Yan, B. Pan, J. Zhou, Y. Xie, *Angew. Chem. Int. Ed.*, 52 (2013) 4361-4365.
21. B. Zheng, R. Yun, J. Bai, Z. Lu, L. Du, Y. Li, *Inorg. Chem.*, 52 (2013) 2823-2829.
22. Z.L. Deng, Q.F. Yi, G. Li, Y. Chen, X.K. Yang, H.D. Nie, *Electrochim. Acta*, 279 (2018) 1-9.
23. S. Zhang, W. Shi, P. Cheng, *Coordin. Chem. Rev.*, 352 (2017) 108-150.
24. X. Zhao, S. Zhang, J. Yan, L. Li, G. Wu, W. Shi, G. Yang, N. Guan, P. Cheng, *Inorg. Chem.*, 57 (2018) 5030-5037.
25. Y. Liu, G. Li, Z. Chen, X. Peng, *J. Mater. Chem. A*, 5 (2017) 9775-9784.
26. S. Chen, S. Liu, A. Wen, J. Zhang, H. Nie, J. Chen, R. Zeng, Y. Long, Y. Jin, R. Mai, *Electrochim. Acta*, 271 (2018) 312-318.
27. C. Li, X. Qiu, K. Deng, Z. Hou, *Anal. Methods*, 6 (2014) 9078-9084.
28. H. Peng, Z. Mo, S. Liao, H. Liang, L. Yang, F. Luo, H. Song, Y. Zhong, B. Zhang, *Sci. Rep.*, 3 (2013)1765.
29. H. Song, A. Tang, G. Xu, L. Liu, M. Yin, Y. Pan, Int. *J. Electrochem. Sci.*, 13 (2018) 4720-4730.
30. C. Wang, Z. Ma, Y. Wang, C. Lu, *J. Electrochem. Soc.*, 163 (2016) A1157-A1163.
31. J. Yin, G.C. Zhu, B.L. Deng, *Desalination*, 379 (2016) 93-101.
32. W.J. Lee, H.R. Jang, M.J. Kim, H.M. Kim, J.M. Oh, S.M. Paek, *J. Alloys Compd*, 778 (2019) 382-390.
33. L. Yang, Y. Feng, D. Yu, J. Qiu, X.F. Zhang, D. Dong, J. Yao, *J. Phys. Chem. Solids*, 125 (2019) 57-63.
34. Q. Yi, Y. Zhang, X. Liu, Y. Yang, *Sci. Chi. Chem.*, 57 (2014) 739-747.
35. J. Tang, W. Gong, T. Cai, T. Xie, C. Deng, Z. Peng, Q. Deng, *RSC Adv.*, 3 (2013) 2543-2547.
36. L. Xin, R. Li, Z. Lu, Q. Liu, R. Chen, J. Li, J. Liu, J. Wang, *J. Electroanal.Chem.*, 813 (2018) 200-207.
37. Y. Wang, T. Liu, X. Lin, H. Chen, S. Chen, Z. Jiang, Y. Chen, J. Liu, J. Huang, M. Liu, *ACS Sustainable Chem. Eng.*, 6 (2018) 13932-13939.
38. D. Wang, Y. Chen, H. Wang, P. Zhao, W. Liu, Y. Wang, J. Yang, *Appl. Surf. Sci.*, 457 (2018) 1018-1024.
39. M. Jiang, X. Cao, D. Zhu, Y. Duan, J. Zhang, *Electrochim. Acta*, 196 (2016) 699-707.
40. L. Wang, C. Wang, H. Wang, X. Jiao, Y. Ouyang, X. Xia, W. Lei, Q. Hao, *Electrochim. Acta*, 289 (2018) 494-502.
41. L. Xin, Q. Liu, J. Liu, R. Chen, R. Li, Z. Li, J. Wang, *Electrochim. Acta*, 248 (2017) 215-224.
42. J. Huang, F. Hao, X. Zhang, J. Chen, *J. Electroanal. Chem.*, 810 (2018) 86-94.
43. B. Joshi, S. Park, E. Samuel, H.S. Jo, S. An, M.W. Kim, M.T. Swihart, J.M. Yun, K.H. Kim, S.S. Yoon, *J. Electroanal. Chem.*, 810 (2018) 239-247.
44. A.P. Tang, X.Y. Wang, S.Y. Yang, J.Q. Cao, *J. Appl. Electrochem.*, 38 (2008) 1453-1457.
45. Q. Yi, W. Yu, *J. Electroanal. Chem.*, 633 (2009) 159-164.

46. Q. Yi, J. Zhang, A. Chen, X. Liu, G. Xu, Z. Zhou, *J. Appl. Electrochem.*, 38 (2008) 695-701.
47. Y. Zhang, Q. Yi, Z. Deng, X. Zhou, H. Nie, *Catal. Lett.*, 148 (2018) 1190-1201.
48. Q. Yi, Q. Chen, *Electrochim. Acta*, 182 (2015) 96-103.
49. Q. Yi, H. Chu, M. Tang, Z. Yang, Q. Chen, X. Liu, *J. Electroanal.Chem.*, 739 (2015) 178-186.
50. Q. Yi, H. Chu, M. Tang, Y. Zhang, X. Liu, Z. Zhou, H. Nie, *Fuel Cells*, 14 (2014) 827-833.
51. Q. Yi, F. Niu, L. Song, X. Liu, H. Nie, *Electroanal.*, 23 (2011) 2232-2240.
52. Y. Zheng, L. Zhang, P. He, D. Dang, Q. Zeng, J. Zeng, M. Liu, *Electrocatal.*, 9 (2018) 495-504.